Nuclear Instruments and Methods in Physics Research B 306 (2013) 99–103

Contents lists available at SciVerse ScienceDirect

Nuclear Instruments and Methods in Physics Research B

journal homepage: www.elsevier.com/locate/nimb

Use of STIM for morphological studies of microstructured polymer foils

E.M. Stori [a,b], C.T. de Souza [a,b], L. Amaral [a], D. Fink [c,d], R.M. Papaléo [e], J.F. Dias [a,b,*]

[a] Ion Implantation Laboratory, Institute of Physics, Federal University of Rio Grande do Sul, Av. Bento Gonçalves 9500, P.O. Box 15051, 91501-970 Porto Alegre, RS, Brazil
[b] Graduate Program of Materials Science, Federal University of Rio Grande do Sul, Av. Bento Gonçalves 9500, P.O. Box 15051, 91501-970 Porto Alegre, RS, Brazil
[c] Departamento de Fisica, Universidad Autónoma Metropolitana-Iztapalapa, P.O. Box 55-534, 09340 México, D.F., Mexico
[d] Nuclear Physics Institute, 25068 Řež, Czech Republic
[e] Faculty of Physics, Catholic University of Rio Grande do Sul, Av. Ipiranga 6681, 90619-900 Porto Alegre, RS, Brazil

ARTICLE INFO

Article history:
Received 25 July 2012
Received in revised form 27 September 2012
Available online 9 November 2012

Keywords:
Scanning transmission ion microscopy
Proton beam writing
Ion beam imaging techniques
Scanning electron microscopy

ABSTRACT

In this work, morphological characterization of microstructures produced by focused 3 MeV H^+ beams and chemical etching on poly(ethylene terephthalate) foils was investigated by on- and off-axis scanning transmission ion microscopy (STIM). STIM images were obtained from different energy regions of the transmitted energy spectra. STIM performance was compared to scanning electron microscopy (SEM) used as a reference. STIM and SEM images provided similar morphological information. The deviations observed between the measured dimensions obtained from both techniques were within the uncertainties of the experiment. Moreover, the scaling of the structures' size versus etching time (i.e. the etching rates) extracted from STIM and SEM data were equivalent. Prolonged etching times of up to 60 min were performed to check the effect of the irradiation on the non-bombarded vicinity of the structured lines. STIM images clearly revealed a distribution of cavities and porosity along the structured walls for etching times above 20 min. This is attributed to thermal effects and outgassing during the proton beam writing, which probably create voids that are enlarged by the long exposure to the etching solution.

1. Introduction

Proton beam writing (PBW) is an important technique for patterning of materials such as glasses, polymers or semiconductors at high spatial resolution [1]. It has found applications in many areas, such as microfluidics, microphotonics, filtering, physiology and tissue engineering among others [2–5]. Scanning transmission ion microscopy (STIM) is a powerful tool for *in situ* morphological characterization of such structures due to its sensitivity to local mass density and thickness. In a homogeneous substrate, this technique can contrast the fabricated structures from the non-irradiated portion of the sample, thus enabling the determination of their dimensions and geometry [6–9]. Besides STIM, Scanning electron microscopy (SEM) is an important tool for morphological studies of polymers irradiated with high energy ions [10]. Despite the undisputable advantages of SEM, one of the drawbacks is that the sample must be coated with carbon or metals like gold because of the insulating properties of polymers. In this case, STIM could be used instead, since it does not require any further sample preparation.

STIM image formation is based on the energy loss contrast between different areas of the sample that are scanned by a focused MeV ion beam. Different strategies for image formation are employed. For instance, strategies based on the energy averaging technique or median filtering technique can lead to images with reduced noise [6]. Another imaging technique uses windowing of the transmitted energy spectrum, taking into account only those ions whose energy fall in a pre-selected window. Although it may produce rather noisy images, it may be useful for the analysis of simpler structures [6–9] because of the gain in structural discrimination, as it is demonstrated in this paper.

The main experimental arrangement for STIM measurements is the so called on-axis configuration, in which the detector is positioned directly behind the sample and thus aligned with the beam. In this case, the primary interaction occurs between the projectile and the target electrons, leading to relatively small scattering angles. Beam currents must be considerably reduced in this configuration (to several thousand ions per second) in order to avoid damage of the detector. The drawback with this configuration is that it cannot be combined with other measurements such as micro-PIXE or micro-RBS which require higher currents. This problem can be overcome by using the off-axis configuration, in which an

* Corresponding author at: Ion Implantation Laboratory, Institute of Physics (UFRGS), Federal University of Rio Grande do Sul, Av. Bento Gonçalves 9500, P.O. Box 15051, 91501-970 Porto Alegre, RS, Brazil. Tel.: +55 51 3308 7248.
E-mail address: jfdias@if.ufrgs.br (J.F. Dias).

0168-583X/$ - see front matter © 2012 Elsevier B.V. All rights reserved.
http://dx.doi.org/10.1016/j.nimb.2012.10.024

angle between the sample axis and the detector (typically between 20° and 45°) is established. This arrangement, however, broadens the spectral peaks, since the ion energy loss includes also interactions with target nuclei, compromising energy and thus spatial resolution [11].

In the present work, on- and off-axis STIM are evaluated as a method for characterization of polymer foils microstructured by PBW. The results are compared to those obtained using SEM in order to assess STIM analytical capabilities.

2. Experimental procedure

Polyethylene terephthalate (PET – Mylar®) foils of 1 cm^2 and 12 μm thick were irradiated at room temperature with 3 MeV protons. The microprobe station consists of an Oxford Microbeams® system operating in triplet mode. A fixed fluence of 6×10^{15} ions/cm^2 and currents varying from 100 to 200 pA were employed for pattering lines on the foils. These lines were drawn in a (100×1) pixels pattern, with a step of writing of 1 μm. The beam spot size was typically 2.0×2.5 μm^2. After the irradiation, the samples were submitted to a 6 M NaOH etching solution in a thermal bath at (60 ± 1) °C with continuous magnetic agitation. The etching time varied from 1 up to 60 min.

The samples were analyzed by on- and off-axis STIM, using a 1 MeV H^+ beam. The reduction of the H^+ energy for the STIM measurements allowed a better assessment of buried structures generated in the polymer without compromising the transmission of the ions. Surface barrier detectors (EG&G Ortec, model BU-011-025-100) with energy resolution of about 8 keV for protons were employed in the measurements. The scan area was 150×150 μm^2 with a 256 pixels matrix. For the on-axis measurements, the current was decreased to around 1500 counts/s at the detector and the total integration time was around 6 min. For the off-axis measurements, a beam current of ~30 pA was used and the number of counts per image is similar to that one obtained for the on-axis case. The angle between the off-axis detector and the beam axis was 24°. Finally, the beam current for on-axis STIM analysis was reduced on the source and not by reducing the slits aperture. This procedure maintained the spot size roughly the same as the one used for the PBW and allowed a straightforward comparison between the on- and off-axis measurements.

STIM maps were produced selecting an energy window encompassing 5–30 channels of the transmitted energy spectra and centered at different positions. In this way, one can highlight structures associated to a particular thickness range which may not be visible if the whole energy spectrum is used. Because of the energy windowing, noisy images are produced but with better detail contrast. The measurements of the length and width of the microstructures were performed with the software ImageJ®, which treats digital images from the STIM maps in terms of color depth. One profile along the major axis and three profiles along the minor axis of the structures were generated, and the resulting edges of the spectra were fitted with error functions in order to obtain the length and width of the structured lines. Fig. 1 shows a drawing depicting the major and minor axis and a typical profile obtained through this methodology.

After the STIM measurements, the same samples were coated with carbon films for the SEM analysis with a Jeol JIB4500 microscope. The samples were tilted by either 52° or 25° in order to measure the height of the walls of the microstructured lines and extract the thickness of the foils. The SEM images were also analyzed using the ImageJ® software. In this case, all dimensions were obtained directly from the images without any need of further treatment.

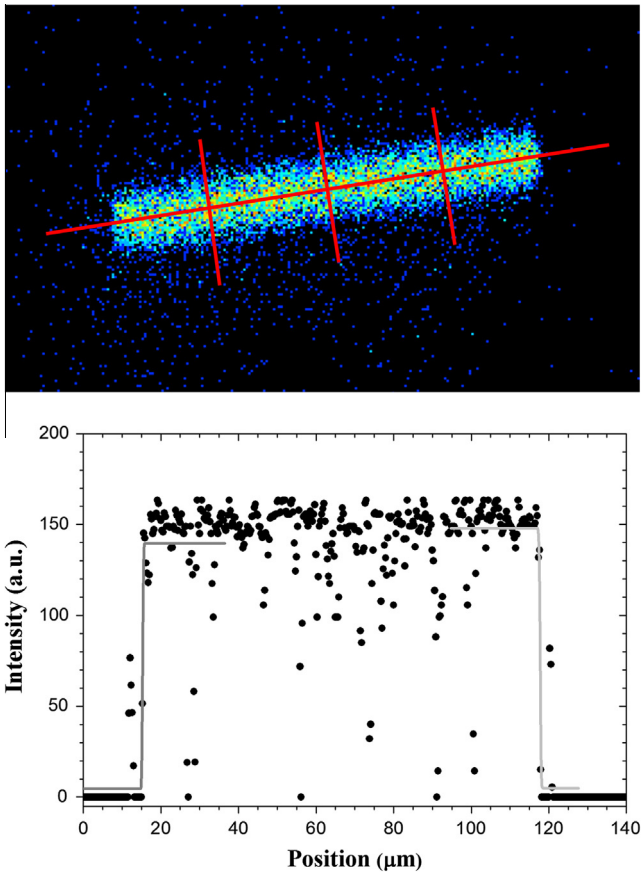

Fig. 1. On-axis STIM image obtained after 10 min of etching. The lines on the top panel represent the major and minor axis from which the profiles were obtained. One typical profile for the major axis is shown with the respective fittings at the edges. The dimensions were calculated from the difference between the centroids of the error (erf) and the complementary error (erfc) functions marked in dark and light gray respectively.

3. Results and discussion

On-axis STIM spectra of all etched samples were characterized by two distinct peaks as shown in Fig. 2. One of them represents the perforation on the sample, i.e. the region where the beam does not loose energy (panel A, energy region D). The lower energy peak (panel A, energy region B) represents the non-irradiated part of the foil where the etching is less effective. In the following discussion, higher and lower energy peaks are referred to as "hole" and "foil" peaks respectively. With increasing etching times, the foil peak approaches the hole peak as expected (panel A in Fig. 3), due to the reduction of the non-irradiated polymer thickness by the etchant. We note that for a sample *not* subjected to post-irradiation etching, the STIM spectrum shows only one broad peak since no hole is directly formed by the writing procedure. In this case, the STIM map obtained by selecting this broad peak shows no contrast in the image. The slight thickness difference at the irradiated line due to sputtering caused by the H^+ beam is apparently too small to be detected in this configuration. By selecting, however, only a narrow shoulder at lower beam energies a STIM map with good contrast at the non-etched bombarded region could also be produced.

STIM maps of etched samples clearly show the hole area, independent of the energy region selected as can be seen in Figs. 2 and 3 (panels B, C and D). The only visible changes are the type of contrast at the hole (negative or positive) and the number of counts of the image. However, additional information could be obtained in samples prepared after longer exposure times to the etchant by selecting the intermediate energy region between the hole and foil

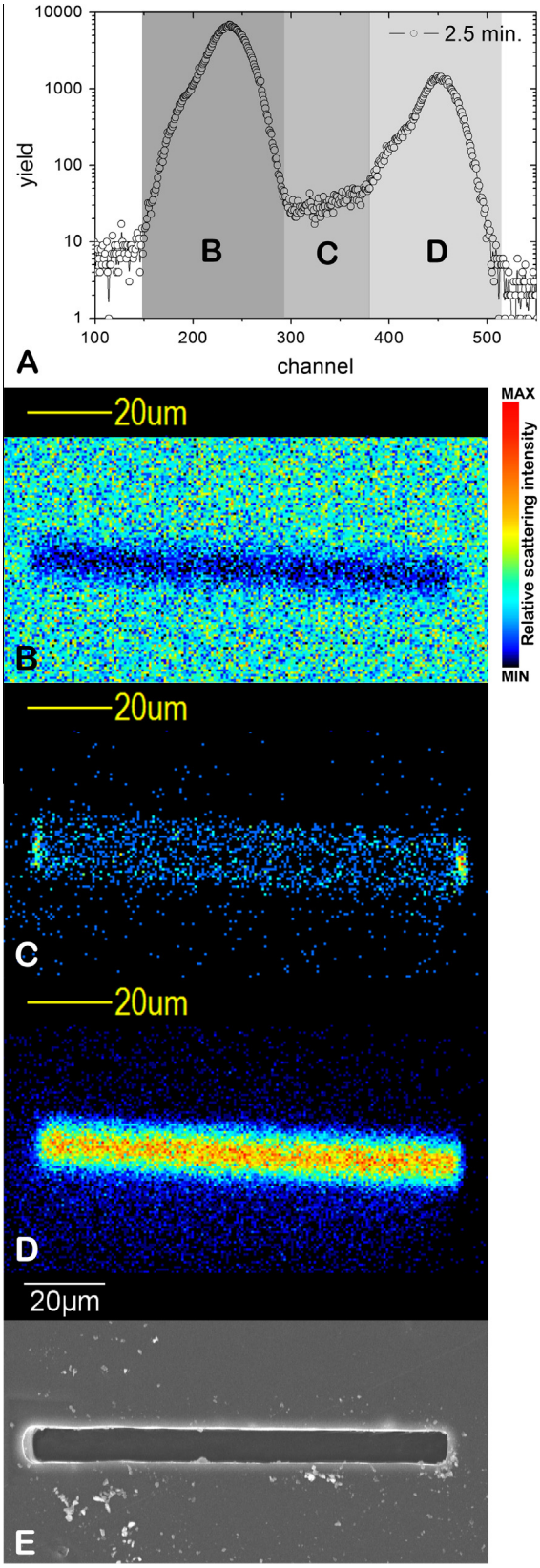

Fig. 2. On-axis STIM and SEM images of a sample structured by PBW and etched for 2.5 min. Panel A depicts the STIM transmission energy spectrum. The low and high energy windows (labels B and D on the energy spectrum) correspond to the "foil" and "hole" peaks and generated the STIM images shown on panels B and D respectively. The intermediate energy window on the energy spectrum (label C) generated the STIM image shown on panel C. Finally, panel E shows the SEM image of the same structure.

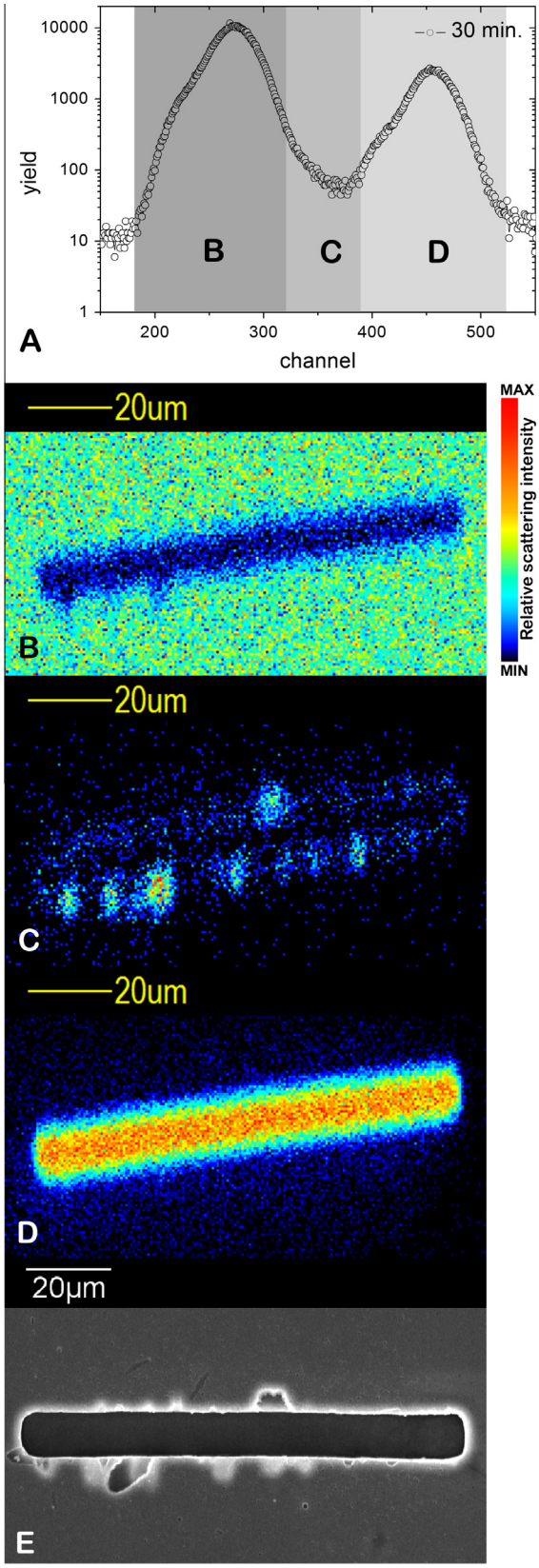

Fig. 3. On-axis STIM and SEM images of a sample structured by PBW and etched for 30 min. Panel A depicts the STIM transmission energy spectrum. The low and high energy windows (labels B and D on the energy spectrum) correspond to the "foil" and "hole" peaks and generated the STIM images shown on panels B and D respectively. The intermediate energy window on the energy spectrum (label C) generated the STIM image shown on panel C. Finally, panel E shows the SEM image of the same structure.

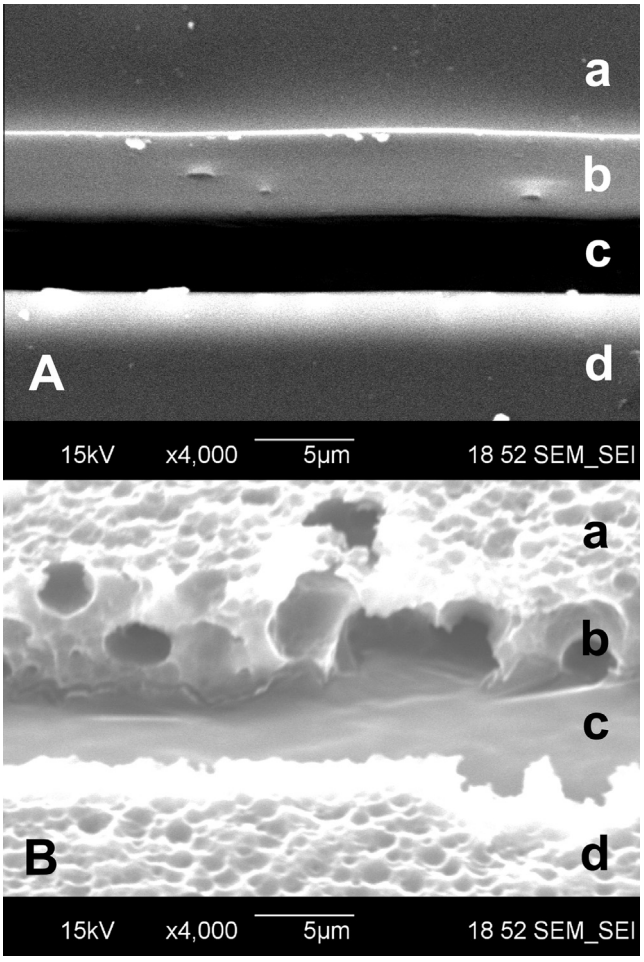

Fig. 4. SEM images depicting the structures obtained after etching times of (A) 1 min and (B) 60 min. These particular images were obtained by tilting the samples to 25°. Portions of the samples marked with a and d correspond to the upper surface of the polymer. Regions b and c correspond to the wall and the bottom of the structures respectively.

peaks. For instance, the STIM image presented in Fig. 3 (panel C) shows the contrast enhancement of cavity-like structures around the patterned lines. These cavities are not clearly seen by STIM if the hole or foil peaks are selected to construct the maps as shown in Fig. 3 (panels B and D). The SEM image shown in Fig. 3 (panel E) also indicates the presence of voids corresponding to those observed on the STIM image of Fig. 3 (panel C). The cavities may be situated on the surface or buried in the polymer. This porous region builds up after long etching times since the etchant starts to attack laterally the walls of the microstructures. This effect is depicted in greater detail in Fig. 4 which shows tilted SEM images zoomed around a microstructured line for two etching times (1 and 60 min). As can be observed in Fig. 4 (panel A), 1 min of etching time was enough to completely remove the material from the irradiated area and keep the walls of the microstructured holes smooth. For longer etching times, several cavities appear on the walls of the structures and over the top surface of the polymer. After 60 min of etching time, a region extending several microns beyond the area of exposure to the microbeam becomes very porous as well, as can be seen in Fig. 4 (panel B). This effect is attributed to excess heating and outgassing during the proton beam writing, which probably create voids that are enlarged by the long exposure to the etching solution.

Off-axis STIM was also performed on the samples for comparison purposes. In this configuration, the scattering energy spectra

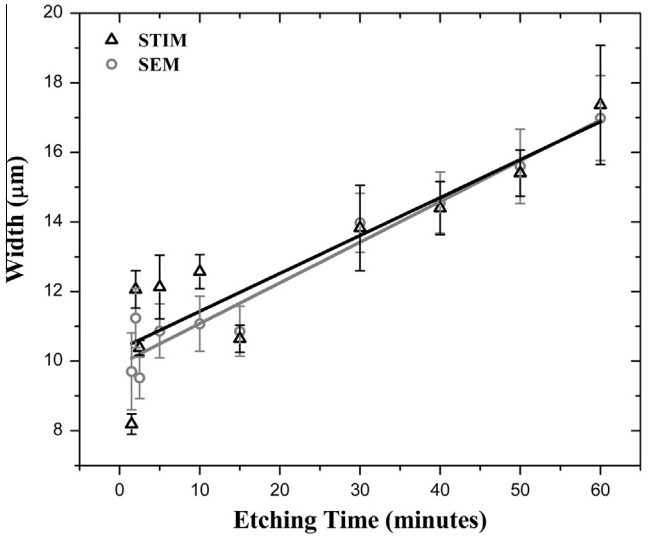

Fig. 5. Width of the structures as a function of the etching time obtained from STIM (triangles) and SEM (circles) images. The black and gray lines stand for linear fittings of the STIM and SEM data respectively. Only data above 1 min of etching time were considered for the fittings. See text for further information.

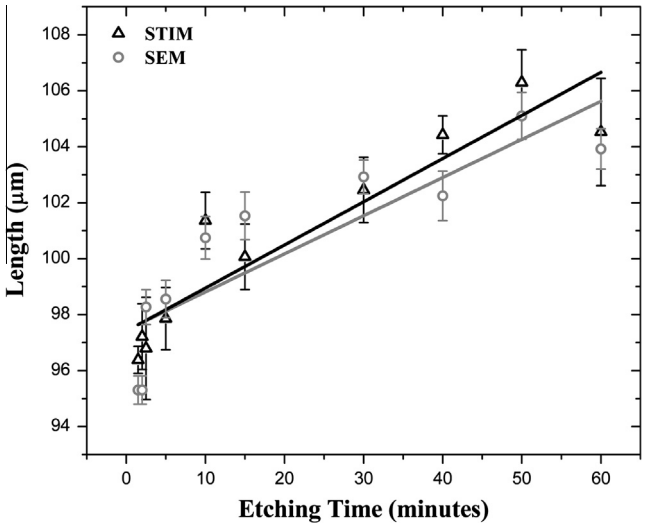

Fig. 6. Length of the structures as a function of the etching time obtained from STIM (triangles) and SEM (circles) images. The black and gray lines stand for linear fittings of the STIM and SEM data respectively. Only data above 1 min of etching time were considered for the fittings. See text for further information.

have rather broad energy peaks. However, with the proper choice of the energy windows, the results obtained are equivalent to those stemming from the on-axis configuration. As off-axis STIM may lead to additional damage because of the larger currents employed, the on-axis configuration is the most suitable for analyzing the microstructured foils.

The results of the STIM and SEM measurements for the width and length of the structures are shown in Figs. 5 and 6 respectively. In general, the dimensions extracted from the STIM and SEM images were compatible with each other. The relatively large fluctuation of the data arises from a combination of different factors affecting the final results. Indeed, the uncertainties related to the PBW procedure itself, the highly-sensitive chemical etching parameters and the fitting procedures of the STIM profile images may lead to such variations. Despite these fluctuations in the

measured values of length and width, the scaling of the structure's size versus etching time (i.e. the etching rates) extracted from STIM and SEM data agree with each other. The etching rates were determined from the slope of a linear fitting of the data for etching times larger than 1 min (solid lines in Figs. 5 and 6). This corresponds to the bulk etching rate of the polymer. Up to 1 min of etching time, the etching rate is much faster since it is related to the polymer region damaged by the beam. Therefore, these data were not included in the fittings. The etching rate along the width of the structures extracted from STIM measurements was 0.11 ± 0.02 μm/min, which is compatible with the value obtained from SEM images (0.12 ± 0.01 μm/min). The same trend was obtained for the evolution of the length of the structured lines since a rate of 0.15 ± 0.02 μm/min and 0.14 ± 0.03 μm/min were extracted from STIM data and SEM images respectively.

4. Conclusions

In this work, the study of PET foils structured through PBW and etching was carried out with STIM and SEM. In particular, on-axis STIM images obtained from different regions of the transmitted energy proved to be a powerful tool for the characterization of buried structures.

STIM and SEM images provided similar morphological information on the microstructured polymer foils. Despite the undisputable advantages of SEM, one of the drawbacks is that the sample must be coated with a conducting layer because of the insulating properties of polymers and it usually has to be measured *ex situ*. STIM may be a good alternative to quickly check the drawn patterns *in situ* without the need of any further sample preparation. Moreover, by carefully choosing the energy window to produce the STIM maps, the contrast of the images are enhanced, revealing different information on the sample structure such as porosity or buried structures. This information cannot be fully assessed by SEM, particularly for deep-buried structures. Therefore, STIM is a useful tool for morphological studies on thin materials structured by PBW.

Off-axis STIM measurements were performed as well in order to compare with those results obtained from the on-axis STIM. In general, the results were equivalent to those obtained with on-axis STIM. However, off-axis STIM provides relatively broader spectral peaks, hampering the analysis of the structures studied in the present work. Therefore, on-axis STIM appears to be a better option for the present case.

Acknowledgment

The authors acknowledge the financial support from the Brazilian agencies CAPES and CNPq.

References

[1] P. Mistry, I. Gomez-Morilla, G.W. Grime, R. Webb, C. Jeynes, R. Gwilliam, A. Cansell, M. Merchant, K.J. Kirkby, Nucl. Instr. Meth. B 231 (2005) 428.
[2] C. Udalagama, E.J. Teo, S.F. Chan, V.S. Kumar, A.A. Bettiol, F. Watt, Nucl. Instr. Meth. B 269 (2011) 2417.
[3] W. Larisch, T. Koal, R. Werner, M. Hohlweg, T. Reinert, T. Butz, Nucl. Instr. Meth. B 269 (2011) 2444.
[4] C.K.M. Ng, V.T. Tjhin, A.C.C. Lin, J.P. Cheng, S.H. Cheng, K.N. Yu, Nucl. Instr. Meth. B 278 (2012) 15.
[5] Y. Furuta, H. Nishikawa, T. Satoh, Y. Ishii, T. Kamiya, R. Nakao, S. Uchida, Nucl. Instr. Meth. B 267 (2009) 2285.
[6] G. Bench, A. Saint, G.J.F. Legge, M. Cholewa, Nucl. Instr. Meth. B 77 (1993) 175.
[7] R. Minqin, J.A. van Kan, A.A. Bettiol, L. Daina, C.Y. Gek, B.B. Huat, H.J. Whitlow, T. Osipowicz, F. Watt, Nucl. Instr. Meth. B 260 (2007) 124.
[8] G.A.B. Gál, I. Rajta, S.Z. Szilasi, Z. Juhász, S. Biri, C. Cserháti, A. Csik, B. Sulik, Nucl. Instr. Meth. B 269 (2011) 2322.
[9] T. Andrea, M. Rothermel, T. Reinert, T. Koal, T. Butz, Nucl. Instr. Meth. B 269 (2011) 2431.
[10] D. Fink, Fundamentals of Ion-Irradiated Polymers, Springer Series in Materials Science, first ed., 2004.
[11] J. Pallon, V. Auzelyte, M. Elfman, M. Garmer, P. Kristiansson, K. Malmqvist, C. Nilsson, A. Shariff, M. Wegdén, Nucl. Instr. Meth. B 219–220 (2004) 988.